Crystallographic analysis on the primary and secondary extension twin variants in Mg alloys

Q L Huang[1], G Chen[2] and R L Xin[2,3]

[1] School of Computer and Information Science, Southwest University, Chongqing, 400715, China
[2] College of Materials Science and Engineering, Chongqing University, Chongqing, 400044, China
[3] Corresponding author.

Email: rlxin@cqu.edu.cn (R. Xin)

Abstract. {10-12}-{10-12} double twins (DTs) are observed in AZ31 Mg alloys after one path uniaxial tension. Secondary twins (STs) are produced mainly from the intersecting points of two primary twins (PTs), forming the PT^{ing}-PT^{ed}-ST grouping. The relative orientations among these variants are analyzed. Statistical analysis reveals that the two primary variants have a specific orientation relationship with the geometric compatibility factor (m') of 0.562. The detwinning of PT^{ed} and ST also have such type of orientation. Moreover, the PT^{ing} and the selected ST have almost opposite shear directions with the angle of 151.1°. Tensor analysis conforms that these geometric orientation relationships are beneficial for minimizing the local strain incompatibility.

1. Introduction

Twinning is an important strain accommodation mechanism for hexagonal close packed (hcp) metals such as Mg, Ti and Zr [1-12]. For Mg alloys, {10-12}<-1011> and {10-11}-<10-1-2> are two most popular twinning modes, which hereafter are referred to as extension twin (ET) and contraction twin (CT), respectively. Under appropriate deformation conditions, secondary twinning can further be activated in primary twins, forming double twins (DTs). For example, {10-11}-{10-12} is the CT-ET type of DTs, which is very popular in AZ31 Mg alloy sheets after rolling at room temperature [1,3-5]. {10-12}-{10-12} is the ET-ET type of DTs, which likely forms in Mg alloys after strain-path change compression. The variant selection of the ET-ET type of DTs have been examined in a previous study [7]. However, it should be addressed that the stress state and hence Schmid factors (SFs) for twinning and dislocation slip are changed when altering the strain path. Moreover, detwinning may become one important deformation mode [13]. These factors largely complicate the analysis of the variant selection rule.

A few studies reported that the ET-ET type of DTs can also be formed in Mg alloys after one path strain deformation [14-19]. In some cases, the applied stress is complicated, which hinders understanding the mechanism of variant selection. Note that knowledge on the selection rule of ET-ET variants in one path deformation is still limited compared to that of CT-ET variants. In recent work [19], we found the formation of {10-12}-{10-12} DTs in AZ31 Mg alloys after simple uniaxial tension at room temperature. The crystallographic aspects of the secondary variants were analyzed and linked to the crystallographic features of the intersecting primary twins. Here, we aim to extend

understanding the selection rule for these variants. Being different from the previous work, here the relative geometric relationships between the intersecting primary variants and that between one primary variant and the secondary twin are analyzed. Then the selection of secondary variants is explained from the point view of local strain accommodation. Moreover, the displacement gradient tensors associated with the primary and secondary variants are calculated and analyzed. This provides some insights into understanding the activation of these DTs.

2. Material and method

A hot rolled AZ31 Mg alloy plate (~70 mm in thickness) is used as the starting material. Fig. 1a is the typical EBSD map of this plate. The average grain size is determined to be ~32 μm by a linear intercept method. Some grains are larger than 100 μm. A cylindrical tensile sample is machined from the AZ31 plate with the axis direction parallel to the normal direction (ND) of the plate. Then the sample is subjected to uniaxial tension at room temperature and at a strain rate of 10^{-3} s^{-1}. The tensile test is interrupted at ~7%. The microstructure of the deformed sample is shown in Fig. 1b. It is clear that many twins are formed in the deformed sample. At the intersecting points of some primary twins (PTs), secondary twins (STs) are produced in the thicker PTs. All the primary and secondary twins are confirmed to be of {10-12}<-1011> type.

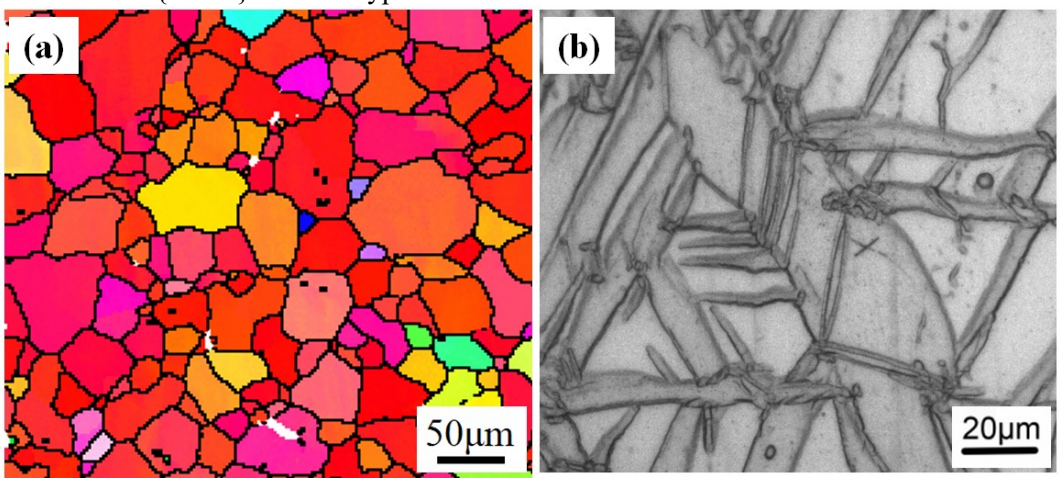

Figure 1. (a) EBSD map showing the original microstructure, (b) Metallurgical graph showing the deformed microstructure.

Due to the hexagonal crystal symmetry, each PT has six crystallographically equivalent variants. There are three types of relative orientations among the six variants [20]. As shown in Fig. 2, these relative orientations are referred to as ortho-position (OP), meta-position (MP) and para-position (PP), respectively [21]. For OP, the angles between the two habit plane normals (ψ) and between the two shear directions (κ) are 40.0° and 42.8°, respectively. Thus, the geometric compatibility factor (defined as $m' = \cos\psi \cos\kappa$) is ~0.562. In previous studies, m' has been used to evaluate the local strain accommodation between slip and twins [22-26]. The m' value ranges from -1 to 1. The larger the m' means the better the local strain compatibility. The ψ, κ and m' for the other types of relative orientations are also calculated, as shown in Fig. 2b. It reveals that the m' for MP and PP is very small, being 0.060 and -0.004, respectively. Previous studies indicated that the variants with OP orientation likely form in the same grain to reduce the local plastic anisotropy. As revealed in Fig. 1b and some previous work [14-16], STs likely initiate from the intersecting points of two PTs. Hereafter, the one containing ST is referred to as PT^{ed} (meaning this PT is impinged by another one); another is referred to as PT^{ing} (meaning this PT is impinging another one). These two PTs together with the ST form a PT^{ing}-PT^{ed}-ST grouping. In the following analysis, the ET variants 1-6 correspond to the indices of (10-12)-[-1011], (01-12)-[0-111], (-1102)-[1-101], (-1012)-[10-11], (0-112)-[01-11], (1-102)[-1101], respectively.

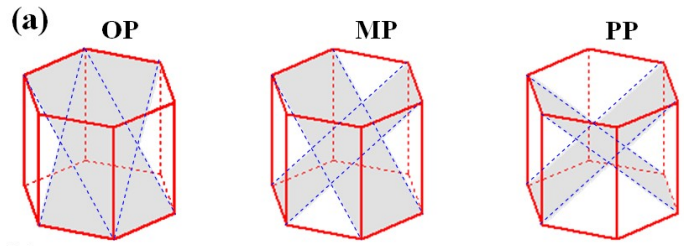

(b)

Geometric Orientations	Ortho-Position (OP)	Meta-Position (MP),	Para-Position (PP)
ψ	40.0°	72.6°	86.3°
κ	42.8°	78.4°	93.7°
m'	0.562	0.060	-0.004

Figure 2. (a) Illustrating the relative orientations of any two variant habit planes, (b) Geometric orientation data between the variants illustrated in (a).

3. Analysis and discussion

The EBSD map in Fig. 3a shows a typical {10-12}-{10-12} DT, where a is the matrix, b, c and d are PTs, and e is a ST formed in b. The ST e is connected with the PT c (or e) at twin b boundary. The unit cells (hexagons) shown in Fig. 3b are constructed based on the Euler angles of a-e. Fig. 3c illustrates the relationships of the different generations of variants. Note that twins c and d have similar orientations and thus correspond to the same variant.

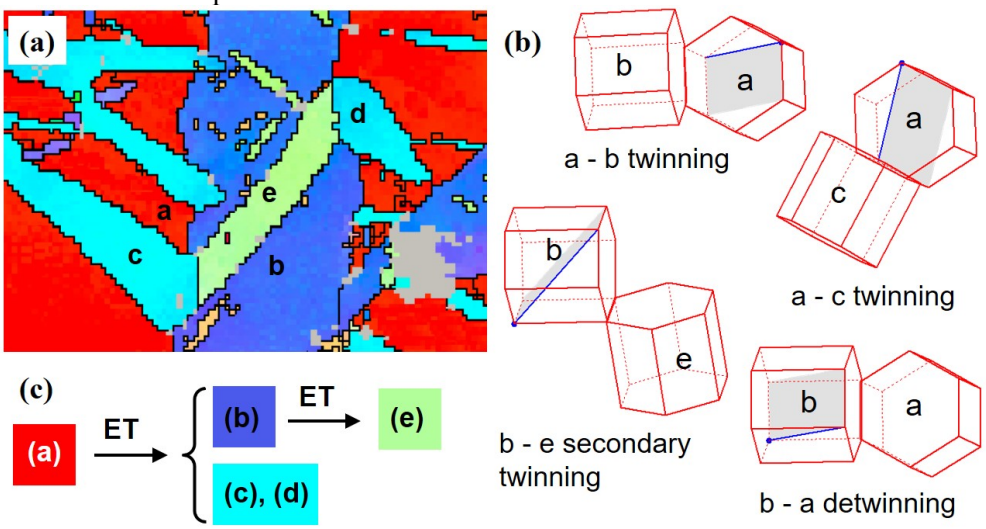

Figure 3. (a) EBSD map showing one typical PT^{ing}-PT^{ed}-ST grouping formed after tension deformation, (b) illustrating the relative orientations between some variants involved the grouping, (c) listing the different generations of twin variants.

The primary and secondary variants are determined based on misorientation analysis. Fig. 4a shows the (0002) stereographic projections for a-d and the six potential PTs. Those for b, e and the six potential STs are shown in Fig. 4b. Here, the potential variant nearest to the observed twin is considered as the active one. In this way, the active twin systems are determined, and their habit planes and shear directions are highlighted in the unit cells as shown in Fig. 3b. It indicates that twins b and c have OP orientation, meaning that their co-activations can minimize the local strain anisotropy. The detwinning of b can be considered as the "twin" a formed in the "matrix" b. Crystallographic

calculations indicate that ψ and κ between detwin b and twin e is 80° and 151.1°, respectively. Therefore, the detwin b also has OP orientation with e. Moreover, as indicated in Fig. 3b, twins c and e have close shear directions. Their angle is calculated to be ~151°. It is worth to mention that the orientation relationship between e and c (or d) is of 49.7°<-909-4>. According to the previous work, this geometric relationship favors the activation of STs in terms of basal slip glide [19].

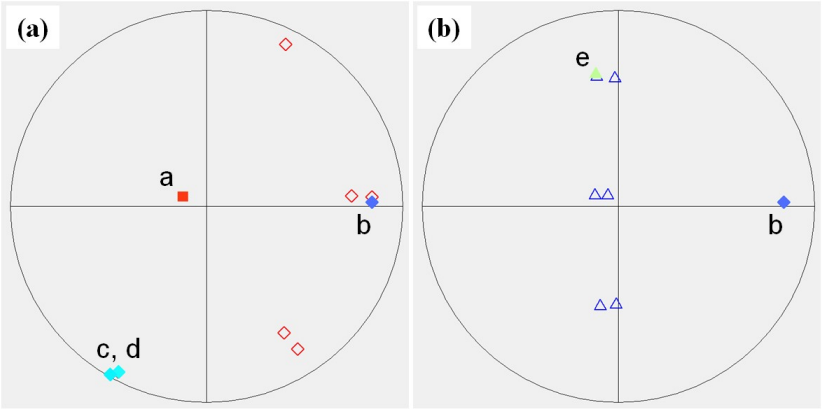

Figure 4. (a) Orientations of twin variants present in Figure 3a: (a) the primary twins, (b) the secondary twins.

Fig. 5a shows the EBSD map of another {10-12}-{10-12} DT. Similarly, b, c and d are PTs, and e is a ST formed in b. The relative orientations of these twin systems are schematic in Fig. 5b. It is seen that twin b has OP orientation with c (or d). Detwin b and twin e also have such kind of orientation. The relationships between the first and second generations of variants are summarized in Fig. 5c. Similar crystallographic analyses are performed on more than 20 PT^{ing}-PT^{ed}-ST groupings. It consistently confirms that the PT^{ing} and PT^{ed} have OP orientation with m'=0.562. The detwinning of PT^{ed} and ST also have such relative orientation. These analyses imply that the relative orientation between PT^{ing} and PT^{ed} and that between PT^{ed} detwin and ST determine the selection of secondary variants. Such kind of grouping is beneficial for minimizing the local strain incompatibility.

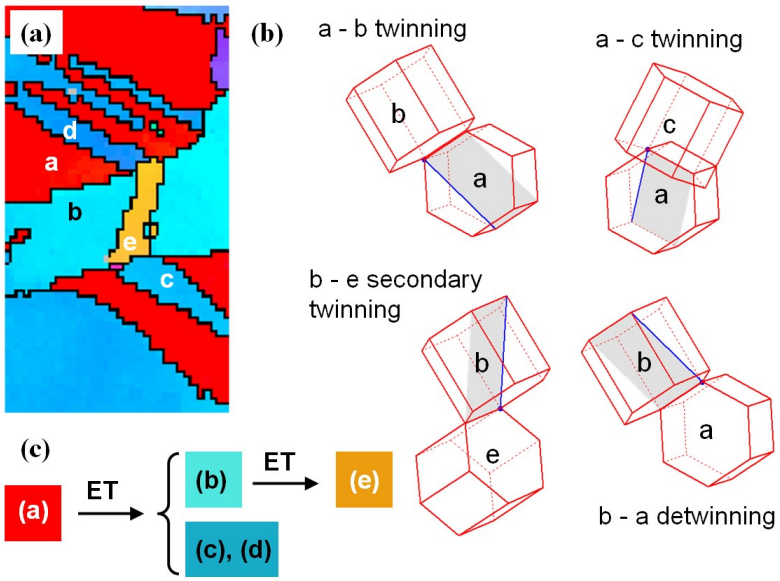

Figure 5. (a) EBSD map showing another PT^{ing}-PT^{e}d-ST grouping formed after tension deformation, (b) illustrating the relative orientations between some variants involved the grouping, (c) listing the different generations of twin variants.

As illustrated in Table 1, six potential STs can be formed in PT_1 (the PT^{ed}). There are 36 relative orientations between the potential ST and PT_1 detwin or the other PTs (i.e. PT_2-PT_6). The ψ, κ and m' for the 36 combinations are calculated and listed in Table 1. In our experiment, more than 90% of the observed PT^{ing}-PT^{ed}-ST groupings have ψ, κ and m' of 80.0°, 151.1° and -0.15, respectively. This corresponds to the combinations of PT_2-ST_{12} or PT_6-ST_{16} in Table 1. According to the indices of twin variants, PT_2 (or PT_6) has OP orientation with PT_1. Similarly, ST_{12} (or ST_{16}) has OP relationship with PT_1 detwin. In addition, Table 1 indicates that the angles between the shear directions of ST_{12} and PT_2 (or of ST_{16} and PT_6) is close to 180°. This implies that the formation of ST and PT^{ing} pairs is helpful to minimize the strain incompatibility at PT^{ed} boundary. On the other hand, the angle between the habit plane normals of ST and PT^{ing} is less important for determining the secondary variants.

Table 1. The theoretical orientation relationships (ψ, κ and m') between PTi and PT1j.

	PT1	PT2	PT3	PT4	PT5	PT6
ST11	0.0 180.0 -1.00	40.0 137.2 -0.56	72.7 101.6 -0.06	86.3 86.3 0.00	72.7 101.6 -0.06	40.0 137.2 -0.56
ST12	40.0 137.2 -0.56	**80.0** **151.1** **-0.15**	108.0 111.1 0.11	101.5 72.8 -0.06	66.9 64.0 0.17	28.9 94.4 -0.07
ST13	72.7 101.6 -0.06	108.0 111.1 0.11	145.3 83.1 -0.10	136.7 40.6 -0.55	96.9 23.3 -0.11	66.9 64.0 0.17
ST14	86.3 86.3 0.00	101.5 72.8 -0.06	136.7 40.6 -0.55	172.6 7.4 -0.98	136.7 40.6 -0.55	101.5 72.8 -0.06
ST15	72.7 101.6 -0.06	66.9 64.0 0.17	96.9 23.3 -0.11	136.7 40.6 -0.55	145.3 83.1 -0.10	108.0 111.1 0.11
ST16	40.0 137.2 -0.56	28.9 94.4 -0.07	66.9 64.0 0.17	101.5 72.8 -0.06	108.0 111.1 0.11	**80.0** **151.1** **-0.15**

The strain accommodation between twinning and dislocation glide has been assessed by tensor analysis. As reported in literature [4], the displacement gradient tensor for ET in Mg alloy is $\begin{bmatrix} 0 & 0 & 0.129 \\ 0 & 0 & 0 \\ 0 & 0 & 0 \end{bmatrix}$. This is expressed in the coordinate system (CS) formed by the shear direction (SD), shear plane normal (SPN) and habit plane normal (HPN). Knowing the twin variant and the orientations of twins and the matrix, this tensor can be transformed to any twin or matrix CS. Then the required strain accommodation can be analyzed. For the PT^{ing}-PT^{ed}-ST grouping shown in Fig. 3a, the tensors associated with the six potential PT_i are transformed to the CS of PT^{ed} (i.e. twin b). Similarly, those associated with the six potential ST_j are transformed in this CS as well. The calculation results are listed in Table 2. The calculated SFs for various variants are also given. In Table 2, c and d correspond to v1 and e corresponds to v4. It is clear that twin e has a small SF of -0.059, implying its formation is not favored by the applied stress. According to literature [4], the components of e_{13} and e_{23} in the tensor of $\begin{bmatrix} e_{11} & e_{12} & e_{13} \\ e_{21} & e_{22} & e_{23} \\ e_{31} & e_{32} & e_{33} \end{bmatrix}$ can be accommodated primarily by basal slip in the CS considered (here it is PT^{ed}). Instead, the components of e_{21} and e_{31} require the strain accommodation from prismatic slip. The tensors in Table 2 reveal that the local strains generated by c (or d) and e requires the strain accommodation mainly from basal slip. Considering the critical resolved shear stress (CRSS) for basal slip is relatively small, the selection of these variants are preferred. Moreover, the absolute

values of $e_{13} + e_{23}$ are close for c (or d) and e, and their signs are of opposite. This implies that the co-activation of PT^{ing} and ST can partly cancel the accommodation strain required from basal slip. This is in agreement with the m' analysis reported in previous work [19].

Table 2. The displacement gradient tensors associated with PT^{ing} and ST expressed in the PT^{ed} crystal frame for the grouping shown in Figure 3b.

PT-SF		PT-Tensor	ST-SF		ST-Tensor
V1 (c, d)	**0.468**	$\begin{pmatrix} -0.021 & 0.107 & \mathbf{-0.043} \\ -0.007 & 0.035 & \mathbf{-0.014} \\ -0.007 & 0.035 & -0.014 \end{pmatrix}$	V1	-0.068	$\begin{pmatrix} -0.064 & 0 & -0.069 \\ 0 & 0 & 0 \\ 0.06 & 0 & 0.064 \end{pmatrix}$
V2	0.455	$\begin{pmatrix} 0.015 & 0.03 & -0.036 \\ 0.025 & 0.049 & -0.059 \\ 0.028 & 0.053 & -0.064 \end{pmatrix}$	V2	-0.475	$\begin{pmatrix} -0.016 & -0.028 & -0.034 \\ -0.028 & -0.048 & -0.059 \\ 0.03 & 0.052 & 0.064 \end{pmatrix}$
V3	0.458	$\begin{pmatrix} -0.021 & -0.008 & 0.01 \\ 0.101 & 0.039 & -0.049 \\ 0.037 & 0.014 & -0.018 \end{pmatrix}$	V3	-0.164	$\begin{pmatrix} -0.016 & 0.028 & 0.034 \\ 0.028 & -0.048 & -0.059 \\ -0.03 & 0.052 & 0.064 \end{pmatrix}$
V4	0.465	$\begin{pmatrix} -0.027 & -0.011 & -0.008 \\ 0.103 & 0.041 & 0.031 \\ -0.045 & -0.018 & -0.014 \end{pmatrix}$	**V4 (e)**	**-0.059**	$\begin{pmatrix} -0.064 & 0 & \mathbf{0.069} \\ 0 & 0 & \mathbf{0} \\ -0.06 & 0 & 0.064 \end{pmatrix}$
V5	0.427	$\begin{pmatrix} 0.015 & 0.025 & 0.024 \\ 0.029 & 0.048 & 0.046 \\ -0.04 & -0.066 & -0.063 \end{pmatrix}$	V5	-0.454	$\begin{pmatrix} -0.016 & -0.028 & 0.034 \\ -0.028 & -0.048 & 0.059 \\ -0.03 & -0.052 & 0.064 \end{pmatrix}$
V6	0.432	$\begin{pmatrix} -0.015 & 0.105 & 0.035 \\ -0.005 & 0.032 & 0.011 \\ 0.008 & -0.052 & -0.017 \end{pmatrix}$	V6	-0.151	$\begin{pmatrix} -0.016 & 0.028 & -0.034 \\ 0.028 & -0.048 & 0.059 \\ 0.03 & -0.052 & 0.064 \end{pmatrix}$

4. Conclusions

Statistical analysis is performed on the PT^{ing}-PT^{ed}-ST groupings formed in AZ31 Mg alloys after tensile deformation. The following major conclusions can be drawn:

(1) The two primary variants (PT^{ing} and PT^{ed}) in the groupings likely form OP orientation with ψ and κ being 40.0° and 42.8°, respectively. This corresponds to a m' of 0.562, the largest one among the three possible values.

(2) The detwining of PT^{ed} and ST also have OP orientation, indicating the groupings of these variants are beneficial for minimizing the local strain anisotropy.

(3) PT^{ing} and the selected ST almost have opposite shear directions (with the angle of 151.1°), implying that the local strain generated by these two variants can be partly cancelled. The extra accommodation strain might be provided by basal slip.

Acknowledgements

This project was supported financially by the National Natural Science Foundations of China (Project No. 51571045 and 51421001).

References

[1] Barnett M, Keshavarz Z, Beer A and Ma X 2008 *Acta Mater.* **56** 5
[2] Koike J, Sato Y and Ando D 2008 *Mater. Trans.* **49** 2792
[3] Martin É, Capolungo L, Jiang L and Jonas J 2010 *Acta Mater.* **58** 3970
[4] Jonas J, Mu S, Al-Samman T, Gottstein G, Jiang L and Martin E 2011 *Acta Mater.* **59** 2046
[5] Luo J, Godfrey A, Liu W and Liu Q 2012 *Acta Mater.* **60** 1986
[6] Mu S, Jonas J and Gottstein G 2012 *Acta Mater.* **60** 2043

[7] Shi Z, Zhang Y, Wagner F, Juan P, Berbenni S, Capolungo L, Lecomte J and Richeton T 2015 *Acta Mater.* **83** 17
[8] Wang S, Schuman C, Bao L, Lecomte J, Zhang Y, Raulot J, Philippe M, Zhao X and Esling C 2012 *Acta Mater.* **60** 3912
[9] Qin H and Jonas J 2014 *Acta Mater.* **75** 198
[10] Xu S, Toth L, Schuman C, Lecomte J and Barnett M 2017 *Acta Mater.* **124** 59
[11] Bingert J, Mason T, Kaschner G, Maudlin P and Gray G 2002 *Metall. Mater. Trans.* A **33** 955
[12] McCabe R, Proust G, Cerreta E and Misra A 2009 *Int. J. Plast.* **25** 454
[13] Xu S, Liu T, Chen H, Miao Z, Zhang Z and Zeng W 2013 *Mater. Sci. Eng.* A **565** 96
[14] Roberts E and Partridge P 1966 *Acta Metall.* **14** 513
[15] Jain J, Zou J, Sinclair C and Poole W 2011 *J. Microsc.* **242** 26
[16] Bian M and Shin K 2013 *Met. Mater. Int.* **19** 999
[17] Jager A, Ostapovets A, Molnár P and Lejček P 2011 *Philos. Mag. Lett.* **91** 537
[18] Suh B, Shim M, Kim D and Kim N 2013 *Scripta Mater.* **69** 465
[19] Xin R, Guo C, Jonas J, Chen G and Liu Q 2017 *Mater. Sci. Eng.* A **700** 226
[20] Nave M and Barnett M 2004 *Scripta Mater.* **51** 881
[21] Yu Q, Wang J, Jiang Y, McCabe R, Li N and Tomé C 2014 *Acta Mater.* **77** 28
[22] Wang L, Eisenlohr P, Yang Y, Bieler T and Crimp M 2010 *Scripta Mater.* **63** 827
[23] Wang L, Yang Y, Eisenlohr P, Bieler T, Crimp M and Mason D 2010 *Metall. Mater. Trans.* A **41** 421
[24] Barnett M, Nave M and Ghaderi A 2012 *Acta Mater.* **60** 1433
[25] Xin R, Guo C, Xu Z, Liu G, Huang X and Liu Q 2014 *Scripta Mater.* **74** 96
[26] Guo C, Xin R, Ding C, Song B and Liu Q 2014 *Mater. Sci. Eng.* A **609** 92